
BRAIN VASCULAR AGE PREDICTION USING CEREBRAL BLOOD FLOW VELOCITY AND MACHINE LEARNING ALGORITHMS

A PREPRINT

Anni Zhao

Center for Data Science
Nell Hodgson Woodruff School of Nursing
Emory University
Atlanta, GA 30322, USA
anni.zhao@emory.edu

Alex Bateh

Division of Nephrology
Department of Medicine
University of Alabama at Birmingham
Birmingham, AL 35294 USA
abateh@uab.edu

Tyler Baldrige

Department of Neurology
School of Medicine
University of Kansas Medical Center
Kansas City, KS 66103, USA
tbaldrige@kumc.edu

Sandra Billinger

Department of Neurology
School of Medicine
University of Kansas Medical Center
Kansas City, KS 66103, USA
sbillinger@kumc.edu

Xiao Hu*

Center for Data Science
Nell Hodgson Woodruff School of Nursing
Emory University
Atlanta, GA 30322, USA
xiao.hu@emory.edu

May 19, 2026

ABSTRACT

Defining vascular age in terms of physiological function has become one focal point of the extensive studies to categorize and track chronological age. Transcranial Doppler (TCD) is a method by which cerebral blood flow velocity is measured along the major arteries feeding the human brain. This study aims to use features extracted from TCD to estimate chronological age and assess accelerated aging in subjects with various brain diseases. We predict subjects with various brain diseases to present with accelerated cerebrovascular aging when tested on various regression models trained by healthy subjects. 168 healthy subjects and 277 diseased subjects with bilateral TCD recordings of the middle cerebral artery were analyzed using the Morphological Analysis and Clustering of Intracranial Pressure (MOCAIP) algorithm. MOCAIP-generated features and heart rate variability features were used as input features for regression models to predict the brain vascular age. 66 subjects with acute stroke, 27 subjects with post stroke, 26 subjects with Alzheimer's disease, 23 subjects with mild cognitive impairment, and 135 established subjects were tested against the machine learning model to assess for accelerated cerebrovascular age. The trained model, on average, predicted healthy subjects' cerebrovascular age to be 3.69 years above their chronological age. Subjects with different disease conditions exhibited varying levels of age acceleration. The differences in healthy and diseased subjects' performances suggest that features generated using TCD may be relevant when evaluating accelerated cerebrovascular aging. Moreover, imbalanced datasets have been observed to affect the performance of machine-learning-based brain age prediction models.

*Corresponding author: Xiao Hu.

Keywords Brain vascular age prediction · Cerebral blood flow velocity · Morphological analysis and clustering of intracranial pressure · Cerebrovascular aging

1 Introduction

Brain vascular aging reflects the progressive structural and functional changes in the cerebral vasculature over time, and it is closely associated with cognitive decline, stroke risk, and other neurological disorders. Accurate prediction of brain vascular age can therefore provide a meaningful biomarker for assessing cerebrovascular health beyond chronological age. Furthermore, a reliable machine learning model plays an important role in the assessment of therapeutic outcomes. In recent years, machine learning algorithms have emerged as a powerful tool for brain vascular age prediction because they can capture complex, nonlinear relationships from physiological [1, 2], imaging [3], and multimodal datasets [4]. By learning patterns associated with vascular aging, these methods offer the potential to identify individuals with accelerated vascular aging at an early stage, support personalized risk assessment, and improve preventive interventions. As a result, brain vascular age prediction using machine learning has become a promising direction in precision medicine and computational neuroscience. Various algorithms and morphologies have been adopted for brain age prediction, including convolutional neural network [5], cortical structure [6], and Hidden Markov Model [7]. Furthermore, there are some algorithm specialities adopted for brain age prediction, such as the decentralized algorithm [8] and extreme learning machine framework [9]. However, there is a large amount of heterogeneity in model performance reported between studies using machine learning models. Mainly, the machine learning model will be trained first on the labeled data from healthy subjects, and implemented for brain age prediction for patients with brain diseases. A comprehensive review of the brain vascular age prediction using machine learning models from 2013 to 2024 can be found in [10]. Another review focusing on the UK Biobank for brain age prediction can be found in [11].

Most of the existing research focused on using MRI-based features for brain vascular age prediction. MRI-based features have shown a significant relationship with the brain vascular age. A well-developed brain vascular age prediction model, DeepBrainNet, has been trained using a large set of MRI scans [12]. Features extracted from various physiological signals have also been adopted for brain vascular age prediction using machine learning algorithms. Recent studies suggest that age-related vascular and neurophysiological changes can be quantified from noninvasive physiological signals, including transcranial Doppler cerebral blood flow velocity [13], near-infrared spectroscopy-derived cerebral pulsation, photoplethysmography [14], and EEG [15, 16]. These findings support the feasibility of developing machine-learning models to estimate brain vascular age from cerebral hemodynamic signal features. Photoplethysmogram (PPG) was adopted for brain vascular age prediction using deep convolutional neural networks in [2]. It has been studied that the artificial intelligence-derived photoplethysmography (AI-PPG) age can serve as a biomarker for cardiovascular health [14]. A distribution-aware loss function was first designed to reduce bias from the imbalanced age distribution. However, limited attention has been given to the imbalanced distribution in brain vascular age prediction. In this paper, the cerebral blood flow velocity measured from TCD and the extracted features are adopted for brain vascular age prediction. It has been investigated that cerebral blood flow velocity is an important aging-related physiological signal. The morphological features extracted from the cerebral blood flow velocity are closely related to age and neuropsychological performance [13, 17]. Furthermore, the influence of dataset imbalance has been investigated to highlight the importance of carefully selecting training and testing datasets for brain vascular age prediction.

The paper is organized as follows. Section 2 explains the datasets that were adopted for the training of the machine learning model. Section 3 shows the feature extraction and machine learning algorithms. Section 4 shows the results of the brain vascular age prediction using various machine learning algorithms. Section 5 concludes the paper.

2 Datasets

Currently, we are mainly using the datasets from the University of Kansas, including 168 healthy subjects and 277 subjects with various diseases. There are 26 patients with Alzheimer’s disease (AD), 23 patients with mild cognitive impairment (MCI), 66 patients with acute stroke, 27 patients with post stroke, and 135 patients are established subjects. Established subjects refer to individuals with a family history of brain disease who may have a higher risk of developing brain disease in the future. Currently, the established subjects do not show any apparent pattern associated with brain diseases. The distribution of the healthy subjects and disease subjects are shown from Fig. 1 to 3.

As observed from Fig.1, we can see that for healthy subjects, most of the datasets are distributed in the age range [20, 30] and [60, 80], and for various diseased subjects, most of the datasets are distributed above age 50. It has been observed that the age distribution for healthy and diseased subjects is highly imbalanced. In this case, the property of imbalancing may influence the performance of the machine learning model. To further improve model performance and ensure age-distribution consistency, healthy subjects over 50 years old were selected as the training dataset because

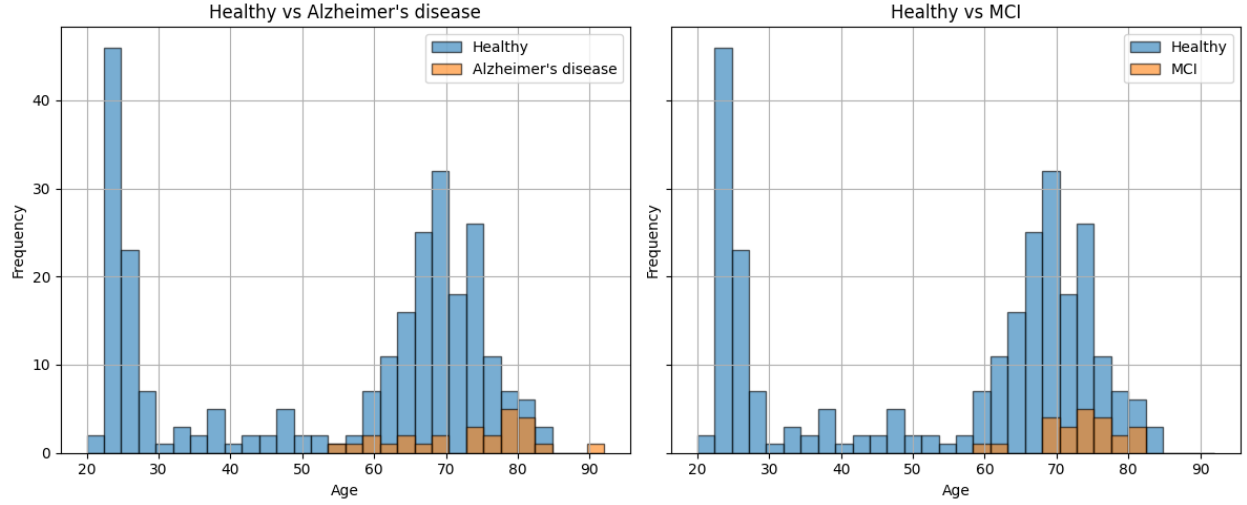


Figure 1: Data distribution of healthy subjects and diseased subjects with Alzheimer's and MCI diseases.

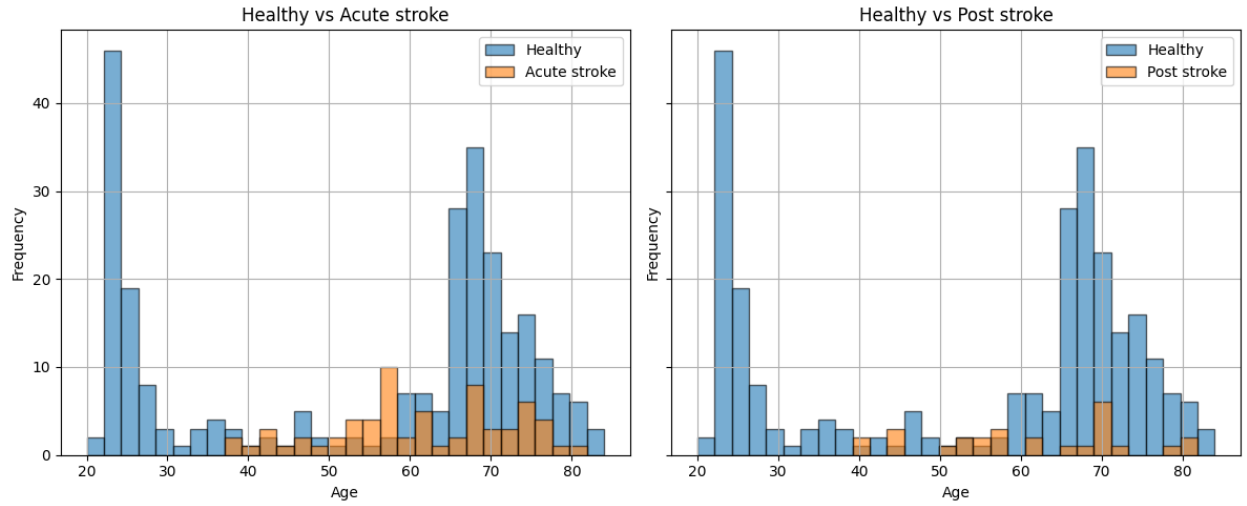


Figure 2: Data distribution of healthy subjects and diseased subjects with acute stroke and post stroke diseases.

most diseased subjects were also older than 50. The distribution of the split training and testing healthy subjects is shown in Fig. 4. 75% of the healthy subjects are adopted as the training datasets, 25% of the healthy subjects are adopted as the testing datasets.

3 Algorithm

In this section, the feature extraction algorithm and machine learning algorithms adopted in this paper are illustrated in detail. The Morphological Clustering and Analysis of the Continuous Intracranial Pressure (MOCAIP) algorithm is adopted to extract the morphological features from the cerebral blood velocity [18]. After feature extraction, the extracted features are served as inputs for the machine learning model, and the age is adopted as the output for the model.

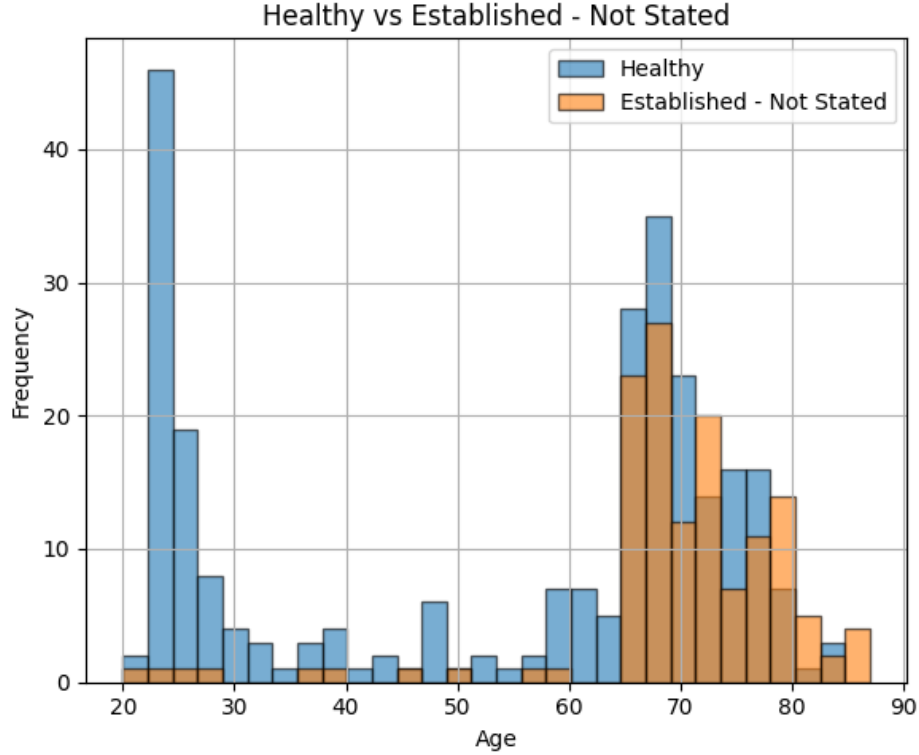


Figure 3: Data distribution of healthy subjects and established subjects.

3.1 Feature extraction algorithm

3.1.1 Pre-analysis

MOCAIP has the ability to extract the dominant pulse from the pulsatile signals. A dominant pulse in the MOCAIP toolbox is the representative pulse waveform selected from a group of pulses in a time window because it best reflects the stable, typical pulse morphology while reducing noise and artifacts. Here, we analyze and compare the averaged dominant pulse across various age groups for healthy subjects as shown in Fig. 5a. It has been observed that as age increases, the amplitude of the dominant pulse decreases with increased waveform complexity. This could be due to the vascular stiffening, wave reflection, and reduced cerebral compliance [19].

Furthermore, the averaged dominant pulse comparisons across the same age group [20, 40] for healthy subjects and diseased subjects are shown from Fig. 5b to 5d. Fig. 5b shows the averaged dominant pulse comparisons in the age group [20, 40] for healthy and acute stroke subjects. Fig. 5c shows the comparisons between the healthy and post stroke subjects. Fig. 5d shows the comparisons between the healthy subjects and established subjects. Higher CBv amplitude and a greater number of waveform peaks were observed in the acute stroke and established groups. These waveform alterations may reflect abnormal cerebrovascular hemodynamics, as TCD-derived CBv waveforms have been shown to provide information related to cerebrovascular occlusion, stenosis, and pathological waveform morphology [20]. Potential physiological mechanisms include impaired or heterogeneous cerebral autoregulation after stroke, compensatory changes in cerebral perfusion, and increased flow through collateral pathways [21]. Moreover, vascular narrowing, disturbed or turbulent flow, and abnormal wave propagation near stenotic vessels may contribute to additional peaks in pulsatile CBv signals [22].

3.1.2 Feature extraction

Fig. 6 shows the data processing in general, including the data selection, signal segmentation, and feature extraction. The 445 entries were selected using the following procedures: (1) data completeness and quality check, and (2) feature validity check. After the data completeness and quality check, signals from each recording were segmented into entries of 360 beats using the MOCAIP toolbox. Each recording is at least 360 beats long. Each entry was then manually reviewed by verifying the validity of the extracted MOCAIP features. There are 128 features in total, and some

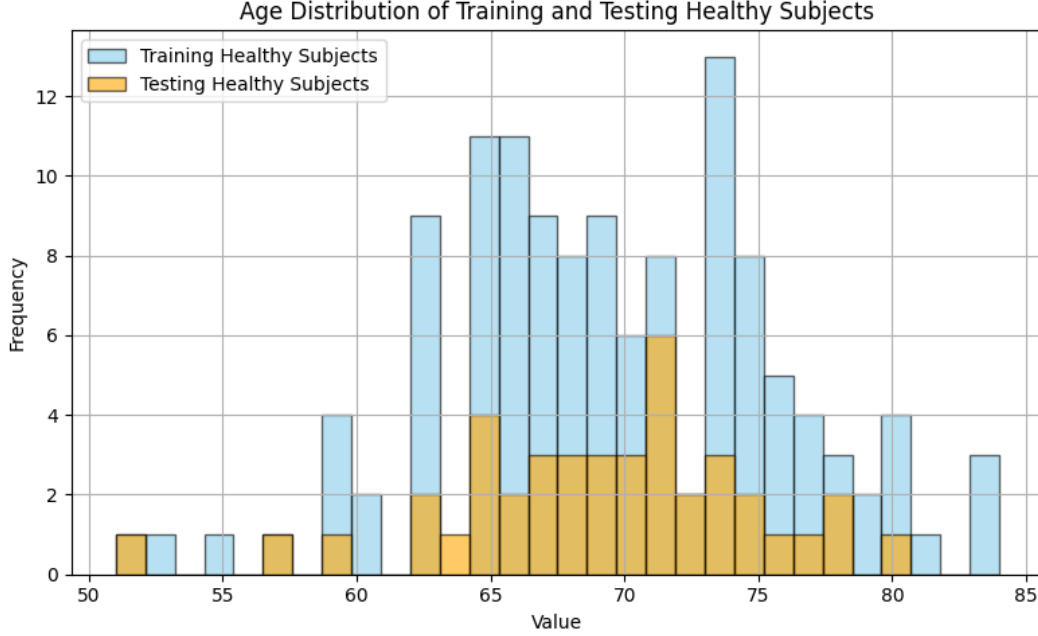


Figure 4: Data distribution of the training and testing healthy subjects for machine learning algorithms.

representative features are shown on the right-hand side of Fig. 6. All datasets, either non-invasive or invasive, are collected synchronously and resampled at 400 Hz. For entries with ECG, the R-R interval is computed using a general biomedical signal processing toolbox for QRS detection. The process of signal segmentation is shown in the middle diagram. The figure and table on the right-hand side show the feature extraction procedure for the MOCAIP toolbox. Other than the 128 features extracted from the MOCAIP toolbox, the body mass index (BMI) and heart rate variability features extracted from the ECG signal are adopted together as a feature vector for the machine learning algorithm. In total, there are 137 numerical features extracted from the TCD and ECG signals. There are various mathematical metrics that have been calculated in MOCAIP. The right-hand side of Fig. 6 shows some representative features, including the amplitude of landmarks from the minimum point, the slope of each rising edge, the mean absolute curvature of the pulse, and the absolute curvature of landmarks. After applying MOCAIP to the healthy and diseased subjects, the top 10 features with the largest group difference are obtained using the variations from the mean value of the features. The features with the largest group difference are computed following the procedures below:

Assume the original feature matrix is

$$X = \begin{bmatrix} x_{11} & x_{12} & \cdots & x_{1p} \\ x_{21} & x_{22} & \cdots & x_{2p} \\ \vdots & \vdots & \ddots & \vdots \\ x_{N1} & x_{N2} & \cdots & x_{Np} \end{bmatrix},$$

where N is the total number of samples and p is the number of features. The element x_{ij} represents the value of the j -th feature for the i -th sample.

If standard scaling is applied, each feature is normalized as

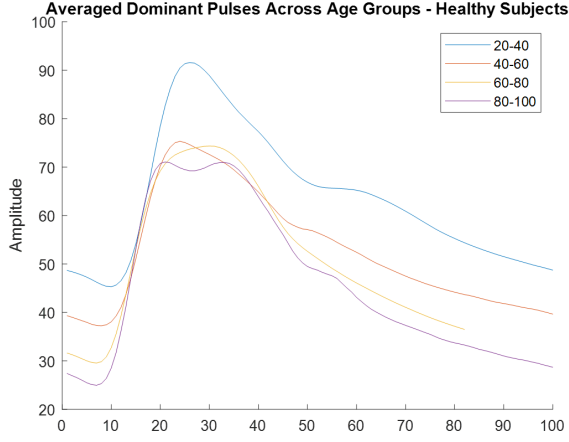
$$z_{ij} = \frac{x_{ij} - \mu_j}{\sigma_j},$$

where μ_j and σ_j are the mean and standard deviation of the j -th feature, respectively. They are defined as

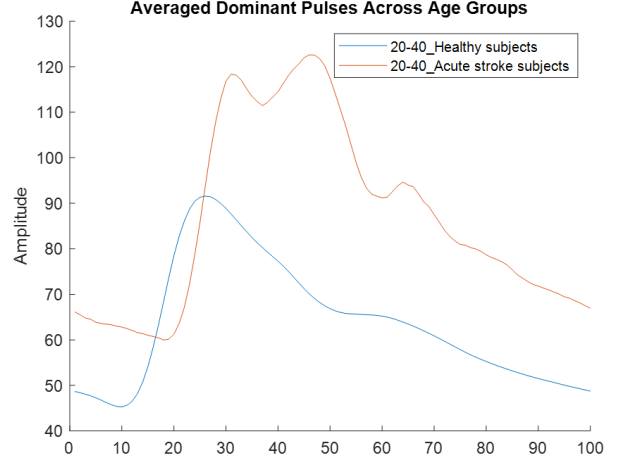
$$\mu_j = \frac{1}{N} \sum_{i=1}^N x_{ij},$$

and

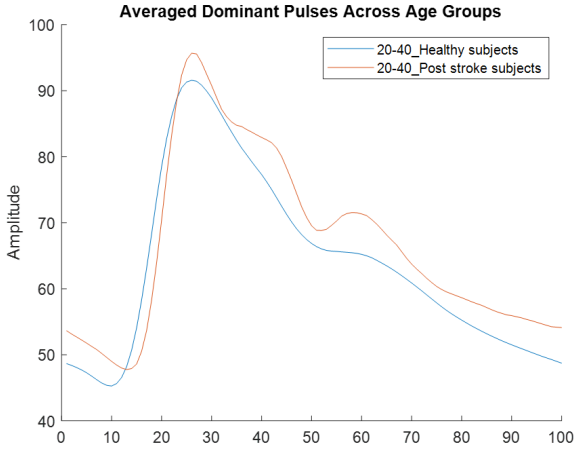
$$\sigma_j = \sqrt{\frac{1}{N-1} \sum_{i=1}^N (x_{ij} - \mu_j)^2}.$$



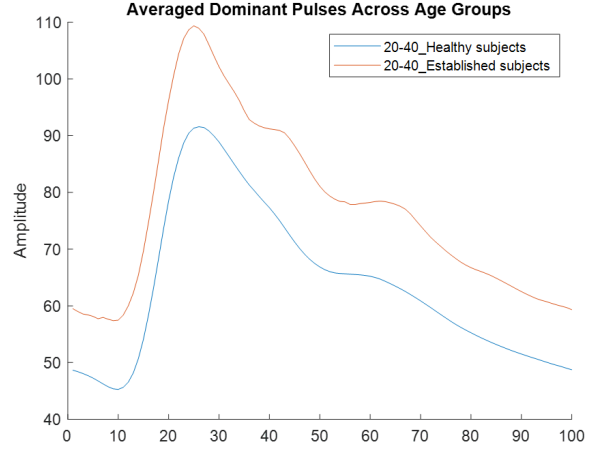
(a) Averaged dominant pulse comparisons across various age groups for healthy subjects.



(b) Averaged dominant pulse comparisons in age group [20,40] for healthy and acute stroke subjects.



(c) Averaged dominant pulse comparisons in age group [20,40] for healthy and post stroke subjects.



(d) Averaged dominant pulse comparisons in age group [20,40] for healthy and established subjects.

Figure 5: Averaged dominant pulse comparisons in age group [20,40] for healthy subjects and different disease groups.

Therefore, the scaled feature matrix can be written as

$$X_{\text{scaled}} = \begin{bmatrix} z_{11} & z_{12} & \cdots & z_{1p} \\ z_{21} & z_{22} & \cdots & z_{2p} \\ \vdots & \vdots & \ddots & \vdots \\ z_{N1} & z_{N2} & \cdots & z_{Np} \end{bmatrix}.$$

Let each sample belong to one of G groups. The group label of the i -th sample is denoted as

$$g_i \in \{1, 2, \dots, G\}.$$

For the g -th group and the j -th feature, the group-wise mean of the scaled feature values is computed as

$$\bar{z}_{gj} = \frac{1}{n_g} \sum_{i:g_i=g} z_{ij},$$

where n_g is the number of samples in group g .

The group-wise feature mean matrix is then given by

$$M = \begin{bmatrix} \bar{z}_{11} & \bar{z}_{12} & \cdots & \bar{z}_{1p} \\ \bar{z}_{21} & \bar{z}_{22} & \cdots & \bar{z}_{2p} \\ \vdots & \vdots & \ddots & \vdots \\ \bar{z}_{G1} & \bar{z}_{G2} & \cdots & \bar{z}_{Gp} \end{bmatrix}.$$

To quantify how much each feature differs across groups, the variance of the group means is calculated for each feature. For the j -th feature, this variance is defined as

$$V_j = \frac{1}{G-1} \sum_{g=1}^G (\bar{z}_{gj} - \bar{z}_{\cdot j})^2,$$

where

$$\bar{z}_{\cdot j} = \frac{1}{G} \sum_{g=1}^G \bar{z}_{gj}$$

is the average of the group means for the j -th feature.

Finally, the features are ranked according to their variance values:

$$V_{j_1} \geq V_{j_2} \geq \cdots \geq V_{j_p}.$$

The top K features are selected as

$$\mathcal{F}_{\text{top}} = \{j_1, j_2, \dots, j_K\},$$

where $K = 10$ in this code. Thus, the selected features are those with the largest variation in group-wise mean values across different groups. The top 10 features obtained are RLp1v2Lp1p2, RLTLp1p3, RLTLv1p2, RLTLp1p2, RLTLv1p3, Lv1p3, LT, RLTLp2p3, RLTLv2p2, and RLv1p1Lv1p3 as defined in MOCAIP. The mathematical definitions [23] of the top 10 features can be found in Table 1. From Table 1 we can see that there is a large group difference in terms of the ratio among time delays, time delay among landmarks, and the time delay between the peaks. A group-level visualization of the standardized features differences can be found in Fig. 7. From Fig. 7, it is observed that the acute stroke patients exhibit significant feature differences compared with the other subject groups. It is interesting to notice that for most of the features there are no large differences between the healthy subjects and the subjects with other diseases. There is minor difference in terms of the time delay among landmarks Lv1p3 for various subjects.

Table 1: Top 10 MOCAIP features with the largest group difference.

Feature	Definition
RLp1v2Lp1p2	Ratio among time delays
RLTLp1p3	Ratio among time delays
RLTLv1p2	Ratio among time delays
RLTLp1p2	Ratio among time delays
RLTLv1p3	Ratio among time delays
Lv1p3	Time delay among landmarks
LT	Time delay of v_1 to ECG QRS peak
RLTLp2p3	Ratio among time delays
RLTLv2p2	Ratio among time delays
RLv1p1Lv1p3	Ratio among time delays

3.2 Machine learning algorithms

Various machine learning algorithms are adopted for the brain vascular age prediction, including the eXtreme Gradient Boosting (XGBoost), CatBoost, Random Forest, Gaussian process regressor, and the Tabular foundation model (TabPFN). XGBoost, CatBoost, and Random Forest are typical tree-based machine learning algorithms. Tree-based ensemble algorithms have been extensively applied in healthcare outcomes prediction, especially for structured clinical data such as EHRs, mortality prediction, readmission, and risk stratification [24]. XGBoost has been applied for predicting 30-days mortality for MIMIC-III patients with sepsis-3 [25] and hospital readmission [26]. Multiple ensemble tree-based algorithms have been adopted for readmission evaluation for stroke patients in [27]. CatBoost has also been extensively applied for dementia risk prediction [28], ICU mortality prediction [29], and carotid sonographic

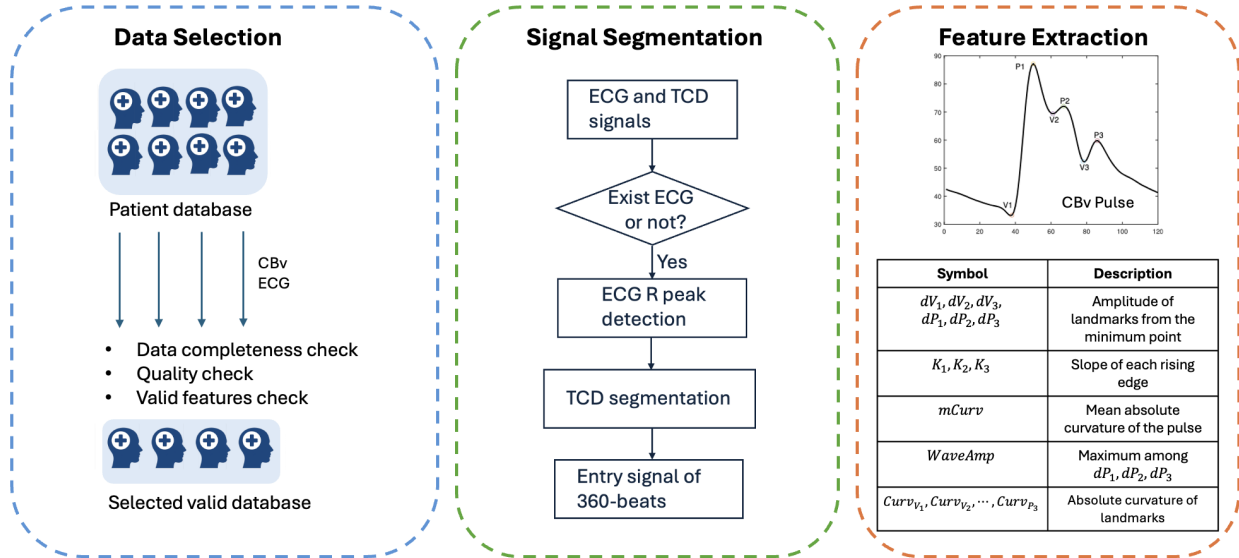


Figure 6: Data processing and feature extraction procedures for brain vascular age prediction using CBv. Left: Data selection procedure from the database. Middle: Signal segmentation for signals with and without ECG. Right: Feature extraction for CBv pulse using MOCAIP.

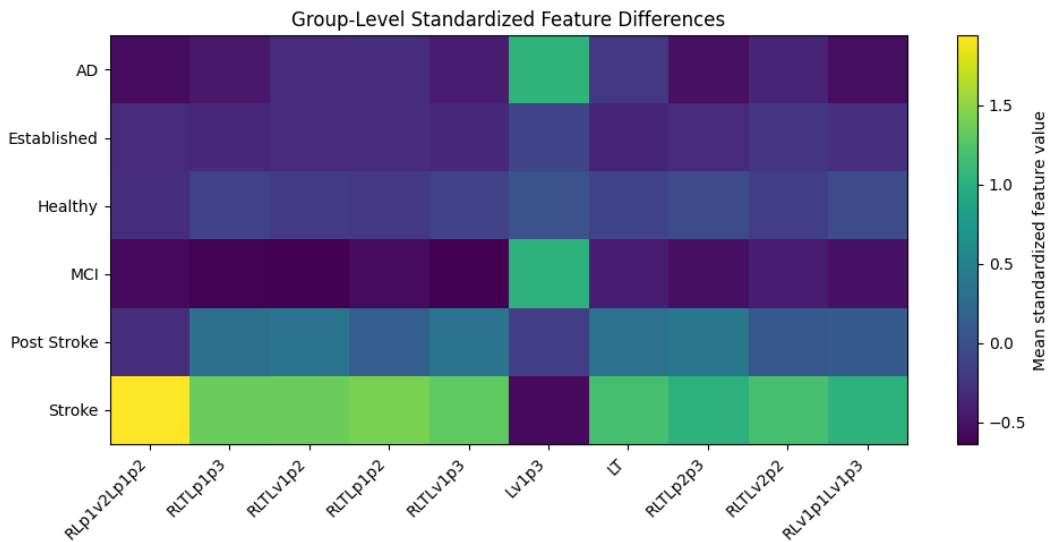


Figure 7: Group-level standardized feature differences for MOCAIP features extracted from the healthy and the diseased subjects.

features analysis for the prediction of recurrent stroke [30]. Random Forest is not as popular as XGBoost and CatBoost. However, it has been applied for dementia-related neuropsychiatric symptoms prediction [31], incident delirium [32], and intensive care unit readmission [33].

Tabular foundation model (TabPFN) [34] is a specific foundation model trained using millions of synthetic tabular datasets. It outperforms the traditional algorithms, such as gradient-boosted decision trees, especially when dealing with datasets with a heterogeneity property. TabPFN has been extensively applied in healthcare [35–37]. [36] proposed an integrated multimodal engine based on TabPFN for image data processing. Recently, TabPFN was also adopted in [35] for lymphovascular invasion prediction in invasive breast cancer. A hybrid LighGBM-TabPFN model was proposed in [37] for dementia prediction in Parkinson’s disease. TabPFN shows significant performance improvement when dealing with smaller tabular datasets and missing values. In this study, the XGBoost, CatBoost, Random Forest, Gaussian process regressor, and TabPFN are adopted for brain vascular age prediction. The MOCAIP and heart rate variability features extracted from the healthy subjects are adopted as inputs, and the age is adopted as output for the machine learning model. After the machine learning model is trained, it is applied to the diseased subjects for early brain disease detection. This approach is based on the assumption that the physiological features extracted from healthy and diseased subjects exhibit distinct characteristics. The healthy subjects are split into training and testing datasets. Furthermore, several resampling strategies were evaluated to address group imbalance; however, they did not consistently improve prediction performance. It has been observed that using healthy datasets above difference age threshold as training datasets yield different results. To guarantee the estimation accuracy, the final model was trained using the healthy subject distributed above age 50 with subgroup-level performance evaluation to assess potential bias across cohorts.

4 Results

The mean absolute errors of the predicted brain vascular age from healthy and diseased subjects for various algorithms are summarized in Table 2. From the results, we can see that the TabPFN yields the smallest mean absolute error of 3.36 for the healthy testing subjects. Moreover, the results from XGBoost, CatBoost, and Random Forest (RF) with balanced sample weighting [38] are included in Table 2. It has been observed that there are minor improvements through incorporating the sample weighting algorithm. The XGBoost with sample reweighting yields the smallest mean absolute error for AD and MCI subjects. The RF with sample reweighting yields the smallest mean absolute error for post stroke and established subjects. Table 3 shows the MAE difference between the healthy subjects and the diseased subjects. It is observed that the XGBoost shows the largest MAE difference between the healthy subjects and the subjects with stroke and established diseases. TabPFN shows the largest MAE difference between the healthy subjects and the subjects with MCI diseases. CatBoost with sample weighting shows the largest MAE difference between the healthy subjects and the subjects with AD and post stroke. On average, AD subjects showed 3.57 years of age acceleration. Patients with MCI showed 1.72 years of acceleration. Stroke patients exhibited the largest age acceleration, with 6.12 years. Post-stroke patients showed 5.51 years of acceleration, while established subjects showed 2.75 years of acceleration. The scatter plot for the predicted brain vascular age from healthy and diseased subjects is shown from Fig. 8 to Fig. 10. Based on the results from Fig. 7, we can see that there are no large feature differences between the subjects with various diseases, which is aligned with the mean absolute error shown in Table 2. The mean absolute errors from the trained machine learning models show no large difference between the subjects with AD, MCI, stroke, post stroke, and established diseases. Table 4 shows the summary of the proportional, standard deviation, and mean of positive brain vascular gaps across various machine learning algorithms. The positive brain vascular age gap is defined as the predicted age minus the chronological age. From Table 4 we can see that the stroke patients show the largest proportional, mean values, and standard deviation for positive brain vascular age gaps. Furthermore, the distribution of the positive predicted age gap and the negative predicted age gap is shown in Fig. 11. From the figure we can see that there are 168 subjects show positive predicted gap and 151 subjects show negative predicted gap. Moreover, most of the positive predicted age gap is distributed in chronological age above 65. Most of the negative predicted age gap is distributed in chronological age below 65. Figs. 12 to 14 shows the chronological age distribution with positive predicted gap and negative predicted gap across different groups. It is observed that for different group, they are following the same distribution - most of the positive predicted age gap is distributed below age 65 ~ 70 and most of the negative predicted age gap is distributed above age 70. This finding may suggest a tendency toward accelerated brain vascular aging among patients older than 65 years.

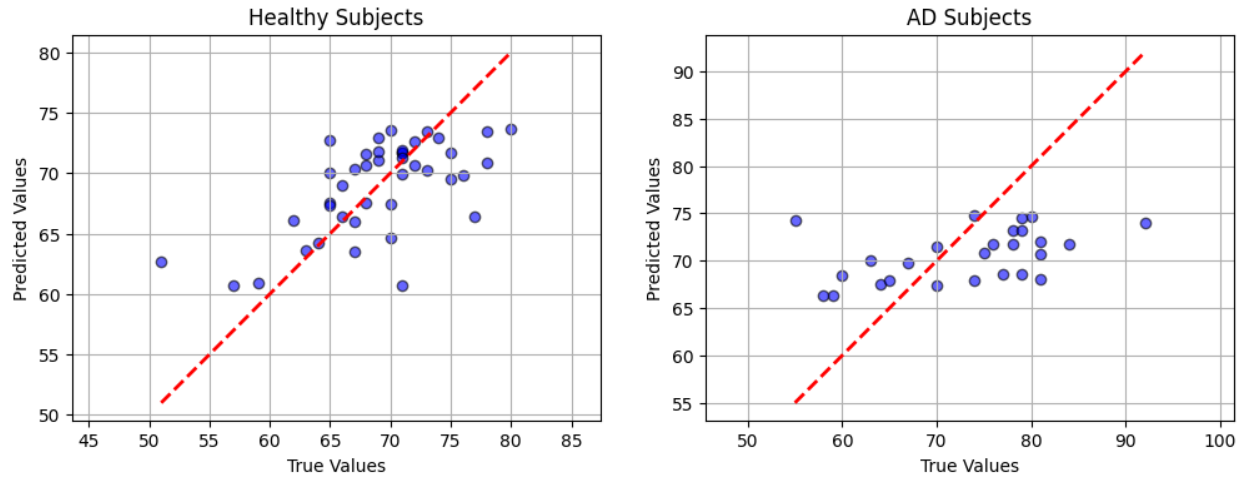


Figure 8: Brain vascular prediction results from healthy and AD subjects.

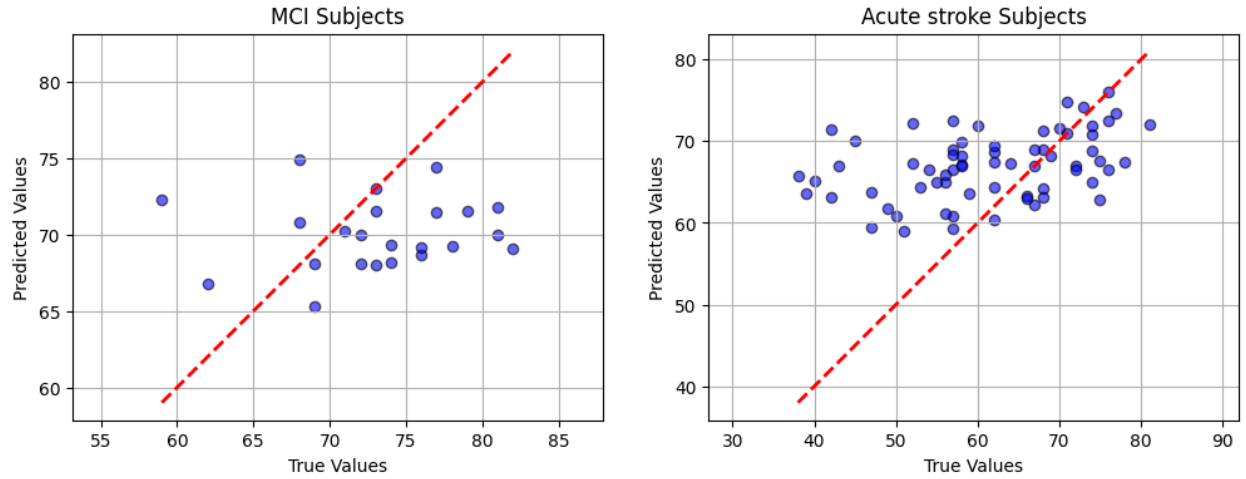


Figure 9: Brain vascular prediction results from subjects with MCI and acute stroke.

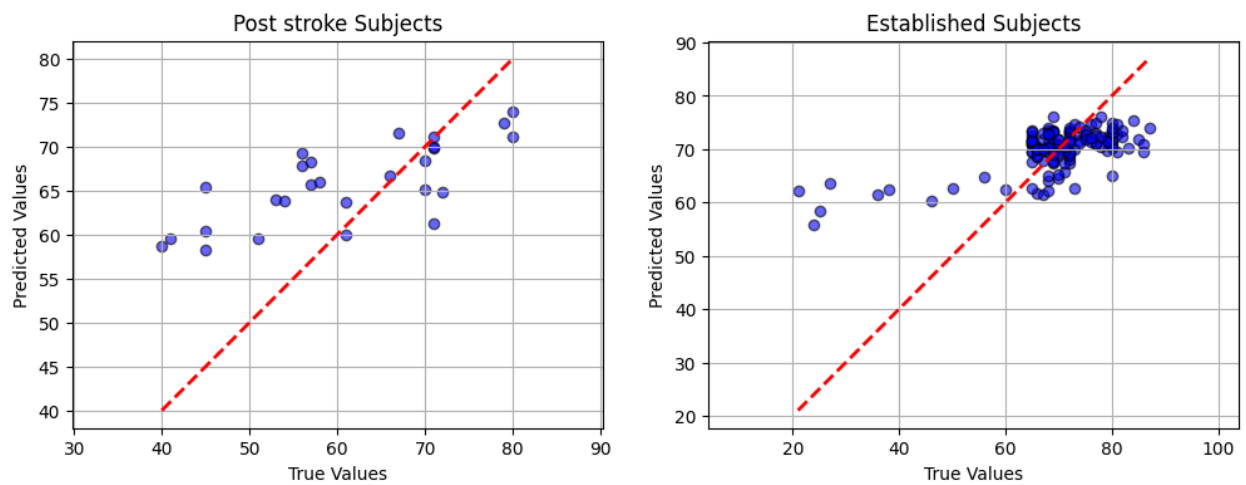


Figure 10: Brain vascular prediction results from post stroke and established subjects.

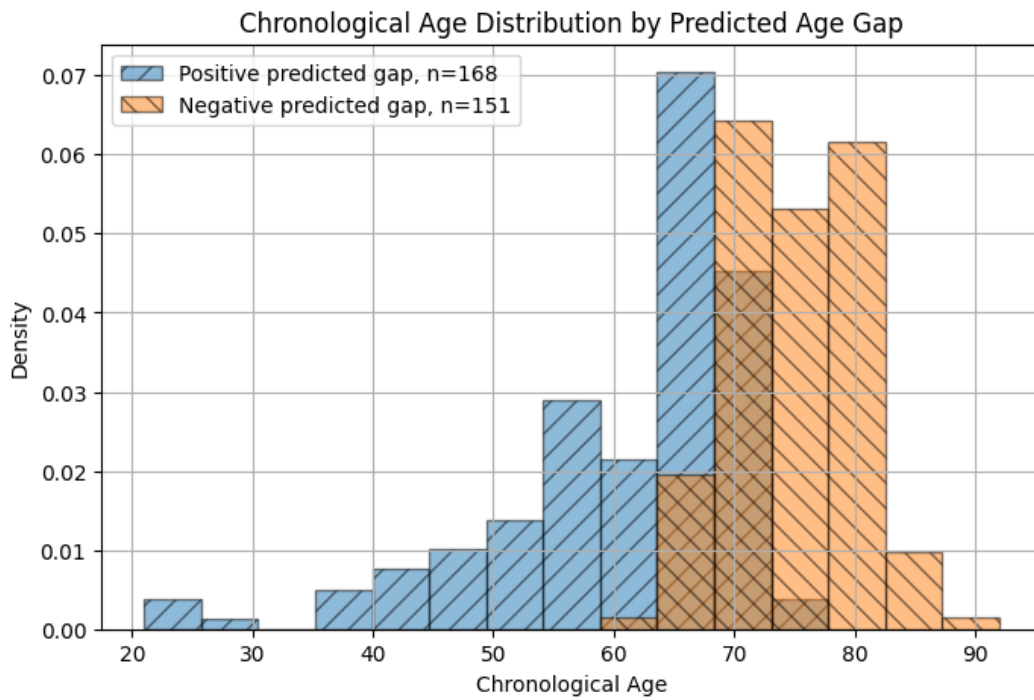


Figure 11: The positive and negative predicted brain vascular prediction gap for all subjects, including the healthy and diseased subjects.

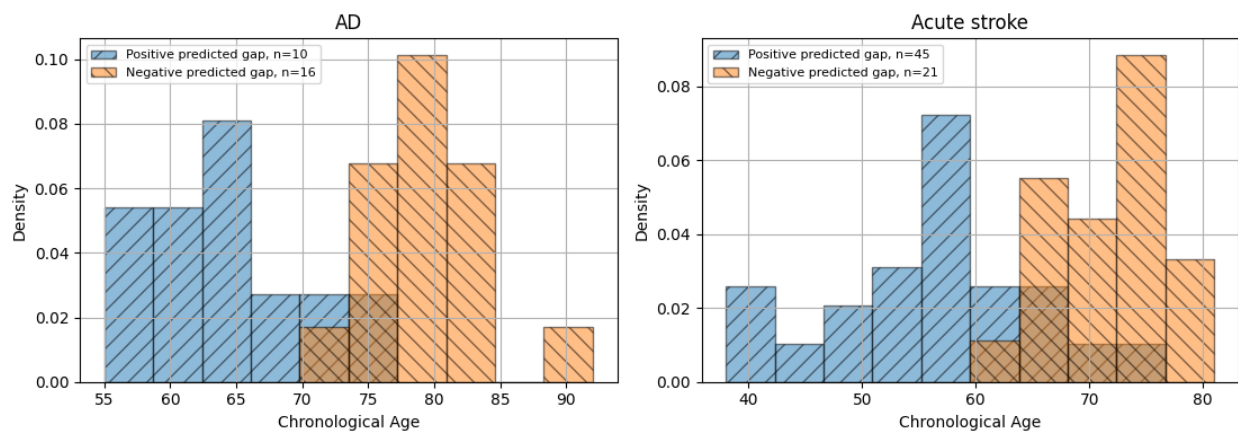


Figure 12: The positive and negative predicted brain vascular age gap for AD and Established subjects.

Table 2: Mean absolute error summary of brain vascular age prediction for healthy and diseased subjects from various machine learning algorithms. The minimum mean absolute error for each machine learning algorithm is highlighted in blue.

Algorithms	Healthy	AD	MCI	Acute stroke	Post stroke	Established
XGBoost	3.78	7.27	4.89	10.24	8.77	6.85
CatBoost	3.70	7.51	5.78	10.00	10.11	6.46
Random forest	3.56	7.24	5.53	9.77	9.82	6.37
XGBoost with sample weighting	4.26	7.03	4.84	10.12	8.90	6.82
CatBoost with sample weighting	3.69	7.51	5.78	10.00	10.11	6.46
RF with sample weighting	3.51	7.19	5.30	9.63	8.32	6.07
TabPFN	3.36	7.12	5.55	8.92	8.39	6.08
Mean	3.69	7.27	5.38	9.81	9.21	6.44

Note: RF denotes random forest.

Table 3: Mean absolute error difference summary of brain vascular age prediction between the healthy and diseased subjects from various machine learning algorithms. The maximum mean error difference for each machine learning algorithm is highlighted in blue.

Algorithms	AD	MCI	Acute stroke	Post stroke	Established
XGBoost	3.49	1.11	6.46	4.99	3.07
CatBoost	3.81	2.08	6.30	6.41	2.76
Random forest	3.68	1.97	6.21	6.26	2.81
XGBoost with sample weighting	2.77	0.84	5.86	4.64	2.56
CatBoost with sample weighting	3.82	2.09	6.31	6.42	2.77
RF with sample weighting	3.68	1.79	6.12	4.81	2.56
TabPFN	3.76	2.19	5.56	5.03	2.72
Mean	3.57	1.72	6.12	5.51	2.75

Table 4: Summary of the proportion, standard deviation, and mean of positive brain vascular age gaps from Tabular foundation model. The groups with the largest proportion, standard deviation, and mean of the brain vascular age gap are highlighted in blue.

Metrics	Healthy	AD	MCI	Stroke	Post stroke	Established
Proportion	0.60	0.38	0.22	0.68	0.67	0.48
Mean	-0.01	-2.51	-3.13	5.67	4.92	0.37
STD	4.36	8.09	5.86	9.98	9.17	9.17

Note: STD denotes standard deviation.

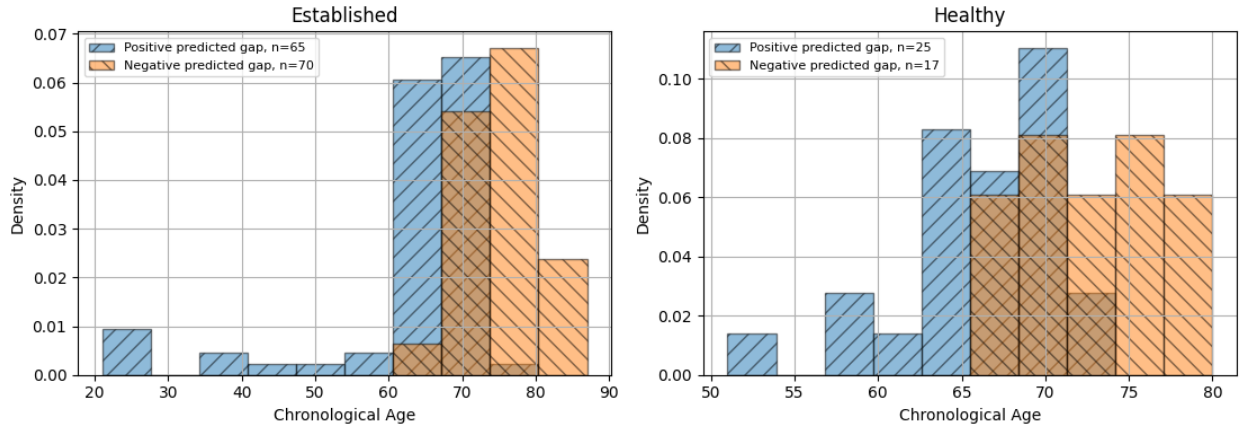


Figure 13: The positive and negative predicted brain vascular age gap for healthy and MCI subjects.

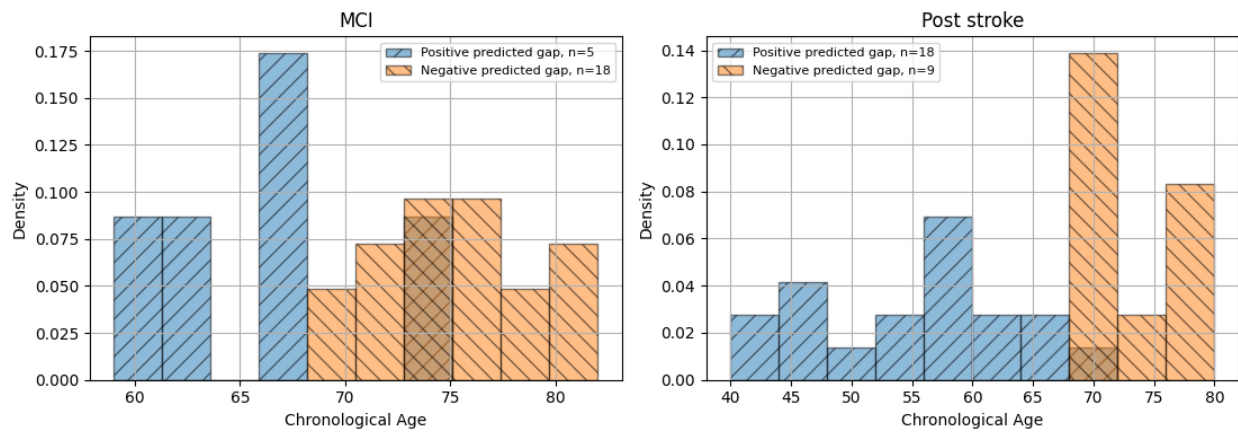


Figure 14: The positive and negative predicted brain vascular age gap for post stroke and stroke subjects.

5 Conclusions

In this paper, the TCD signal is adopted for brain vascular age prediction. Mathematical features extracted using MOCAIP and heart rate variability toolbox are adopted as inputs for the machine learning algorithm. Various machine learning algorithms, including XGBoost, CatBoost, Random Forest, and Tabular foundation model, are adopted for brain vascular age prediction. It has been observed that the Tabular foundation model yields the smallest MAE for testing healthy subjects. XGBoost shows the largest MAE difference for stroke and established subjects, CatBoost shows the largest MAE difference for subjects with AD and post stroke. However, it has been observed that brain vascular age prediction depends heavily on the distribution of the age. In general, the age distribution for healthy subjects is highly imbalanced, and there are limited approaches existing for dealing with imbalanced datasets for brain age prediction. Although balanced sample weighting was adopted in this study to address the imbalanced age distribution, only limited performance improvement was observed. In the future, it is worth investigating a more effective resampling approach for brain vascular age prediction with imbalanced datasets. Furthermore, the unequal sample sizes among diseased groups could introduce bias into the machine learning model predictions. Demographic information, including gender and BMI, along with measurement-related factors such as estimation position, should be considered during the modeling and evaluation of machine learning models.

References

- [1] Julian Libiseller-Egger, Jody E Phelan, Zachi I Attia, Ernest Diez Benavente, Susana Campino, Paul A Friedman, Francisco Lopez-Jimenez, David A Leon, and Taane G Clark. Deep learning-derived cardiovascular age shares a genetic basis with other cardiac phenotypes. *Scientific reports*, 12(1):22625, 2022. ISSN 2045-2322.
- [2] Hangsik Shin, Gyujeong Noh, and Byung-Moon Choi. Photoplethysmogram based vascular aging assessment using the deep convolutional neural network. *Scientific Reports*, 12(1):11377, 2022. ISSN 2045-2322.
- [3] Hongfang Han, Sheng Ge, and Haixian Wang. Prediction of brain age based on the community structure of functional networks. *Biomedical Signal Processing and Control*, 79:104151, 2023. ISSN 1746-8094.
- [4] Tamoghna Chattopadhyay, Pavithra Senthilkumar, Rahul H Ankarath, Christopher Patterson, Emma J Gleave, Sophia I Thomopoulos, Heng Huang, Li Shen, Lei You, and Degui Zhi. Deep learning to predict future cognitive decline: a multimodal approach using brain mri and clinical data. *Frontiers in Neuroimaging*, 5:1726037, 2026.
- [5] Katia Maria Poloni, Ricardo José Ferrari, and Alzheimer’s Disease Neuroimaging Initiative. A deep ensemble hippocampal cnn model for brain age estimation applied to alzheimer’s diagnosis. *Expert Systems with Applications*, 195:116622, 2022. ISSN 0957-4174.
- [6] Christopher R Madan and Elizabeth A Kensinger. Predicting age from cortical structure across the lifespan. *European Journal of Neuroscience*, 47(5):399–416, 2018. ISSN 0953-816X.
- [7] Bing Wang and Tuan D Pham. Mri-based age prediction using hidden markov models. *Journal of neuroscience methods*, 199(1):140–145, 2011. ISSN 0165-0270.
- [8] Sunitha Basodi, Rajikha Raja, Bhaskar Ray, Harshvardhan Gazula, Jingyu Liu, Eric Verner, and Vince D Calhoun. Federation of brain age estimation in structural neuroimaging data. In *2021 43rd Annual International Conference of the IEEE Engineering in Medicine & Biology Society (EMBC)*, pages 3854–3857. IEEE, 2021. ISBN 172811179X.
- [9] Peyman Hosseinzadeh Kassani, Alexej Gossmann, and Yu-Ping Wang. Multimodal sparse classifier for adolescent brain age prediction. *IEEE journal of biomedical and health informatics*, 24(2):336–344, 2019. ISSN 2168-2194.
- [10] LK Soumya Kumari and R Sundarajan. A review on brain age prediction models. *Brain Research*, 1823:148668, 2024. ISSN 0006-8993.
- [11] Yanxue Li, Hongjian Gao, Lan Lin, Yutong Wu, and Xinyu Zhu. Uk biobank-centric advances in brain age prediction: a comprehensive review. *Reviews in the Neurosciences*, 37(1):19–42, 2026. ISSN 0334-1763.
- [12] Vishnu M Bashyam, Guray Erus, Jimit Doshi, Mohamad Habes, Ilya M Nasrallah, Monica Truelove-Hill, Dhivya Srinivasan, Liz Mamourian, Raymond Pomponio, and Yong Fan. Mri signatures of brain age and disease over the lifespan based on a deep brain network and 14 468 individuals worldwide. *Brain*, 143(7):2312–2324, 2020. ISSN 0006-8950.
- [13] Matt L Miller, Paolo Ghisletta, Bradley S Jacobs, Cheryl L Dahle, and Naftali Raz. Changes in cerebral arterial pulsatility and hippocampal volume: a transcranial doppler ultrasonography study. *Neurobiology of Aging*, 108:110–121, 2021. ISSN 0197-4580.

- [14] Guangkun Nie, Qinghao Zhao, Gongzheng Tang, Yaxin Li, and Shenda Hong. Artificial intelligence-derived photoplethysmography age as a digital biomarker for cardiovascular health. *Communications Medicine*, 5(1):481, 2025. ISSN 2730-664X.
- [15] Denis A Engemann, Apolline Mellot, Richard Höchenberger, Hubert Banville, David Sabbagh, Lukas Gemein, Tonio Ball, and Alexandre Gramfort. A reusable benchmark of brain-age prediction from m/eeg resting-state signals. *Neuroimage*, 262:119521, 2022. ISSN 1053-8119.
- [16] Shiang Hu, Xue Xiang, Xiaolong Huang, Yan Lu, Xulai Zhang, Dezhong Yao, and Pedro A Valdes-Sosa. Lifespan brain age prediction based on multiple eeg oscillatory features and sparse group lasso. *Frontiers in Aging Neuroscience*, 17:1559067, 2025. ISSN 1663-4365.
- [17] Matthew P Pase, Natalie A Grima, Con Stough, Andrew Scholey, and Andrew Pipingas. Association of pulsatile and mean cerebral blood flow velocity with age and neuropsychological performance. *Physiology & behavior*, 130:23–27, 2014. ISSN 0031-9384.
- [18] Xiao Hu, Peng Xu, Fabien Scalzo, Paul Vespa, and Marvin Bergsneider. Morphological clustering and analysis of continuous intracranial pressure. *IEEE Transactions on Biomedical Engineering*, 56(3):696–705, 2008.
- [19] Aichi Chien, Fernando Vinuela, Viktor Szeder, Geoffrey Colby, Reza Jahan, Anthony Wang, Satoshi Tateshima, Gary Duckwiler, and Noriko Salamon. Cerebrovascular longitudinal atlas: Changes in cerebral arteries in unruptured intracranial aneurysm patients followed with mra. *NeuroImage: Clinical*, 46:103766, 2025. ISSN 2213-1582.
- [20] Samuel G Thorpe, Corey M Thibeault, Nicolas Canac, Kian Jalaieiddini, Amber Dorn, Seth J Wilk, Thomas Devlin, Fabien Scalzo, and Robert B Hamilton. Toward automated classification of pathological transcranial doppler waveform morphology via spectral clustering. *PloS one*, 15(2):e0228642, 2020. ISSN 1932-6203.
- [21] Hongyin Ma, Zhen-Ni Guo, Hang Jin, Xiuli Yan, Jia Liu, Shan Lv, Peng Zhang, Xin Sun, and Yi Yang. Preliminary study of dynamic cerebral autoregulation in acute ischemic stroke: association with clinical factors. *Frontiers in Neurology*, 9:1006, 2018. ISSN 1664-2295.
- [22] Jongyeol Kim. Pictorial essay: transcranial doppler findings of the intracranial and extracranial diseases. *Journal of Neurosonology and Neuroimaging*, 11(1):2–21, 2019. ISSN 2635-425X.
- [23] Shadnaz Asgari, Nestor Gonzalez, Andrew W Subudhi, Robert Hamilton, Paul Vespa, Marvin Bergsneider, Robert C Roach, and Xiao Hu. Continuous detection of cerebral vasodilatation and vasoconstriction using intracranial pulse morphological template matching. *Plos one*, 7(11):e50795, 2012. ISSN 1932-6203.
- [24] Patrick Doupe, James Faghmous, and Sanjay Basu. Machine learning for health services researchers. *Value in Health*, 22(7):808–815, 2019. ISSN 1098-3015.
- [25] Nianzong Hou, Mingzhe Li, Lu He, Bing Xie, Lin Wang, Rumin Zhang, Yong Yu, Xiaodong Sun, Zhengsheng Pan, and Kai Wang. Predicting 30-days mortality for mimic-iii patients with sepsis-3: a machine learning approach using xgboost. *Journal of translational medicine*, 18(1):462, 2020. ISSN 1479-5876.
- [26] Peng Zhao, Illhoi Yoo, and Syed H Naqvi. Early prediction of unplanned 30-day hospital readmission: model development and retrospective data analysis. *JMIR medical informatics*, 9(3):e16306, 2021.
- [27] Negar Darabi, Niyousha Hosseinichimeh, Anthony Noto, Ramin Zand, and Vida Abedi. Machine learning-enabled 30-day readmission model for stroke patients. *Frontiers in neurology*, 12:638267, 2021. ISSN 1664-2295.
- [28] Huitong Ding, Amiya Mandapati, Alexander P Hamel, Cody Karjadi, Ting FA Ang, Weiming Xia, Rhoda Au, and Honghuang Lin. Multimodal machine learning for 10-year dementia risk prediction: the framingham heart study. *Journal of Alzheimer's Disease*, 96(1):277–286, 2023. ISSN 1387-2877.
- [29] Nima Safaei, Babak Safaei, Seyedhouman Seyedekrami, Mojtaba Talafidaryani, Arezoo Masoud, Shaodong Wang, Qing Li, and Mahdi Moqri. E-catboost: An efficient machine learning framework for predicting icu mortality using the eicu collaborative research database. *Plos one*, 17(5):e0262895, 2022. ISSN 1932-6203.
- [30] Shih-Yi Lin, Kin-Man Law, Yi-Chun Yeh, Kuo-Chen Wu, Jhih-Han Lai, Chih-Hsueh Lin, Wu-Huei Hsu, Cheng-Chieh Lin, and Chia-Hung Kao. Applying machine learning to carotid sonographic features for recurrent stroke in patients with acute stroke. *Frontiers in Cardiovascular Medicine*, 9:804410, 2022. ISSN 2297-055X.
- [31] Javier Mar, Ania Gorostiza, Oliver Ibarrondo, Carlos Cernuda, Arantzazu Arrospide, Álvaro Iruin, Igor Larrañaga, Mikel Tainta, Enaitz Ezpeleta, and Ane Alberdi. Validation of random forest machine learning models to predict dementia-related neuropsychiatric symptoms in real-world data. *Journal of Alzheimer's Disease*, 77(2):855–864, 2020. ISSN 1387-2877.
- [32] John P Corradi, Stephen Thompson, Jeffrey F Mather, Christine M Waszynski, and Robert S Dicks. Prediction of incident delirium using a random forest classifier. *Journal of medical systems*, 42(12):261, 2018. ISSN 0148-5598.

-
- [33] Juan C Rojas, Kyle A Carey, Dana P Edelson, Laura R Venable, Michael D Howell, and Matthew M Churpek. Predicting intensive care unit readmission with machine learning using electronic health record data. *Annals of the American Thoracic Society*, 15(7):846–853, 2018. ISSN 2329-6933.
- [34] Noah Hollmann, Samuel Müller, Lennart Purucker, Arjun Krishnakumar, Max Körfer, Shi Bin Hoo, Robin Tibor Schirrmeyer, and Frank Hutter. Accurate predictions on small data with a tabular foundation model. *Nature*, 637(8045):319–326, 2025. ISSN 0028-0836.
- [35] Yunhua Li, Jianfeng Yang, Pan Xiao, Haibo Liu, Yingjun Zhou, Xiuqi Yang, Gangwen Chen, and Zhichao Zuo. Mri delta-radiomics and morphological feature-driven tabPFN model for preoperative prediction of lymphovascular invasion in invasive breast cancer. *Technology in Cancer Research & Treatment*, 24:15330338251362050, 2025. ISSN 1533-0346.
- [36] Jiaqi Luo, Yuan Yuan, and Shixin Xu. Time: TabPFN-integrated multimodal engine for robust tabular-image learning. *arXiv preprint arXiv:2506.00813*, 2025.
- [37] Vinh Quang Tran and Haewon Byeon. Predicting dementia in parkinson’s disease on a small tabular dataset using hybrid lightgbm–tabPFN and shap. *Digital Health*, 10:20552076241272585, 2024. ISSN 2055-2076.
- [38] Fabian Pedregosa, Gaël Varoquaux, Alexandre Gramfort, Vincent Michel, Bertrand Thirion, Olivier Grisel, Mathieu Blondel, Peter Prettenhofer, Ron Weiss, and Vincent Dubourg. Scikit-learn: Machine learning in python. *the Journal of machine Learning research*, 12:2825–2830, 2011. ISSN 1532-4435.